Is curvature overrated? No, it depends on the geology

Satinder Chopra[1] and Kurt J. Marfurt[2]

Abstract

In an article that appeared in the June 2014 issue of *First Break*, it was suggested that seismic curvature attribute is an overrated attribute and that the coherence attribute was better for carrying out interpretation of discontinuity features such as channels and faults. We believe that coherence and curvature are complimentary attributes that define tectonic deformation including faulting and folding as well as incisement, collapse, and differential compaction of stratigraphic horizons, and add additional insight to the same geologic features being interpreted. Instead of searching for the best attribute or getting into a debate of an attribute being overrated or not, we recommend the complimentary application of these attributes for interpretation of the features of interest, and strongly contend that this aspect not be overlooked.

Introduction

Recently, an article entitled 'Is curvature overrated?' appeared in the June 2014 issue of *First Break*, in which the author compares curvature attributes with discontinuity attributes as well as relative amplitude change attribute, and highlighted a few observations, that included, (1) For routine exploration of faults and channels, discontinuity attributes consistently produce more interpretable images than curvature; (2) Many studies give the impression that curvature is superior to discontinuity for all purposes, which the author disputes; and (3) Curvature attributes reveal finer detail than other attributes, but its significance is unclear and awaits further explanation.

Having spent a fair amount of time on the generation of such attributes and more, and having made attempts to interpret the coherence and curvature attributes for significant discontinuity lineaments, we both feel there is a definite value in each of these attributes in terms of discontinuity detail that they have to offer. While we agree with the observations that the author of the article has shown in his examples, we think the inferiority seen in those examples is geologic rather than algorithmic. As seen by our affiliations, one of us lives in the Western Canadian Sedimentary Basin and the other in the USA 'Midcontinent', giving us a very different perspective from those working Tertiary sand and shale basins such as the Gulf of Mexico, offshore West Africa, or southeast Asia. Specifically, most of our work has dealt with more indurated Mesozoic and Paleozoic rocks, very often with a strong carbonate component, and more recently with a strong mudrock (shale gas and oil reservoir) component. To provide the readership with a broader perspective on the use of seismic attributes in interpretation, we therefore wish to counter Barnes's (2014) observations with some of our own. Our goal is therefore tutorial, with the objective of encouraging greater discussion in this important field of analysis.

Curvature and coherence are two of the more popular 'geometric' attributes. As the name implies, geometric attributes measure changes in reflector shape or morphology. Other geometric attributes include dip magnitude and dip azimuth, energy gradients, amplitude curvature, reflector rotation, and reflector convergence/parallelism. Other commonly used attributes such as RMS amplitude, envelope, spectral components, and impedances are typically computed one trace at a time and while sensitive to changes in morphology (such as lateral changes in tuning thickness) do not directly attempt to measure them. To avoid confusion, one could be more specific in the particular discontinuity attribute that is being used for comparison.

Let us consider the coherence family of attributes first. Coherence is a similarity attribute. There are different algorithms that can be used for generating the coherence attribute, namely, cross-correlation (Bahorich and Farmer, 1995), semblance (Marfurt et al. 1998), eigenstructure (Gersztenkorn and Marfurt, 1999), gradient structure tensor chaos (Bakker, 2003), Sobel filters (Luo et al., 1996), chaos (lateral Hilbert transforms (Luo et al., 2003), and Energy Ratio (Chopra and Marfurt, 2008) algorithms. The differences between these attributes are best understood by examining some end members. For example, let us consider a thin channel that falls below seismic resolution that modifies the reflector

[1] *Arcis Seismic Solutions, TGS, Calgary.*
[2] *University of Oklahoma, Norman.*
[*] *Corresponding author, E-mail: schopra@arcis.com*

amplitude, but not the waveform. Cross-correlation, eigenstructure, and energy ratio coherence algorithms will not see such a fault, since the waveform does not change, while those coherence attributes sensitive to amplitude (semblance, Sobel filter, chaos, and lateral Hilbert transforms) will. In contrast, the paper by Gersztenkorn and Marfurt (1999) evaluating coherence images of deeply incised canyons and faults radiating from a salt dome shows eigenstructure measure to be superior to semblance and cross-correlation measures.

In contrast, curvature measures the lateral change in dip magnitude and dip azimuth. Typically, we assign a positive value to anticlinal shapes and a negative sign to synclinal shapes. Horizontal and dipping planes exhibit a zero value, so our hypothesized thin channel described in the previous paragraph would not be mapped by curvature. Figure 1a from Barnes (2014) summarizes the major features delineated using curvature attributes. He shows how a positive curvature anomaly is associated with the upthrown side

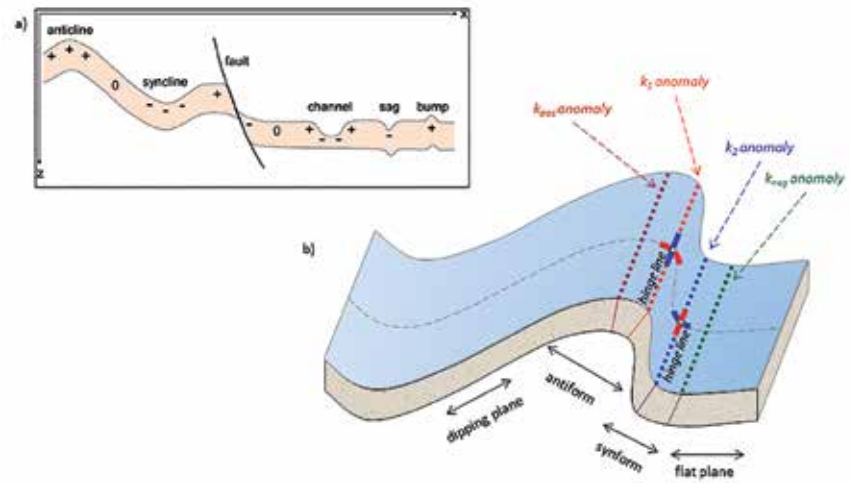

Figure 1 *(a) Sign convention for curvature attributes. Positive curvature reveals anticlines, reflection bumps, flexural highs, negative curvature reveals synclines and reflection sags. In this paper, the curvature colour bar sets positive curvature to red and negative curvature to blue. (After Barnes, 2014). (b) Image showing the difference between crest and trough – the positive and negative hinge lines of a tight fold. The maxima of the second derivative of a time structure map will generate most-positive and most-negative curvature anomalies corresponding to the crest and trough. In contrast, the most-positive and most-negative principal curvatures (k_1 and k_2) anomalies will track the hinge lines which are areas of maximum strain. (After Mai et al., 2009).*

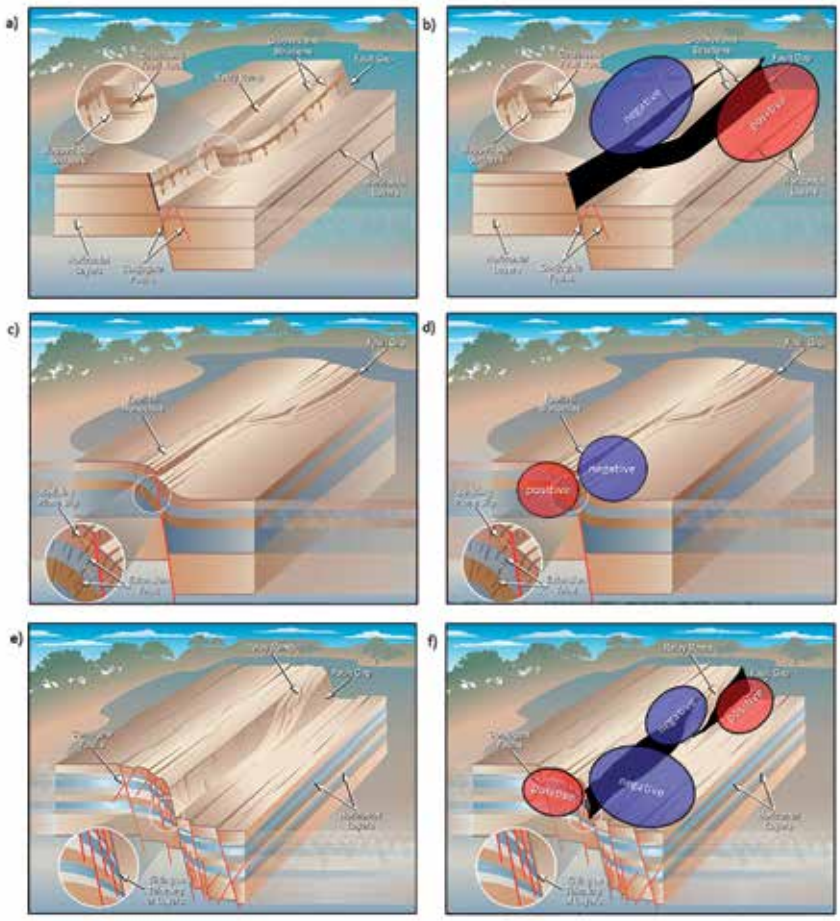

Figure 2 *Images from Ferrill and Morris (2008) summarizing fault expression seen at the Beckman Limestone Quarry, Texas within the (a) Edwards Group, (c) Eagle Ford Formation, and (e) Glen Rose Formation. Cartoons of fault attribute expression showing (b) a strong coherence anomaly due to fault displacement along a horsetail fault with weak curvature anomalies (large radius circles) associated with the relay ramp, (d) strong curvature anomalies (small radius circles) but no coherence anomaly of a fault giving rise to strong bedding plane slip, and (f) coherence anomalies associated with displacement along an en echelon fault and curvature anomalies due to conjugate faults giving rise to tilting and thinning of layers. There are also strong curvature anomalies associated with the relay ramp that transfers strain from one fault to the next. AAPG©[2008], reprinted by permission of the AAPG whose permission is required for further use.*

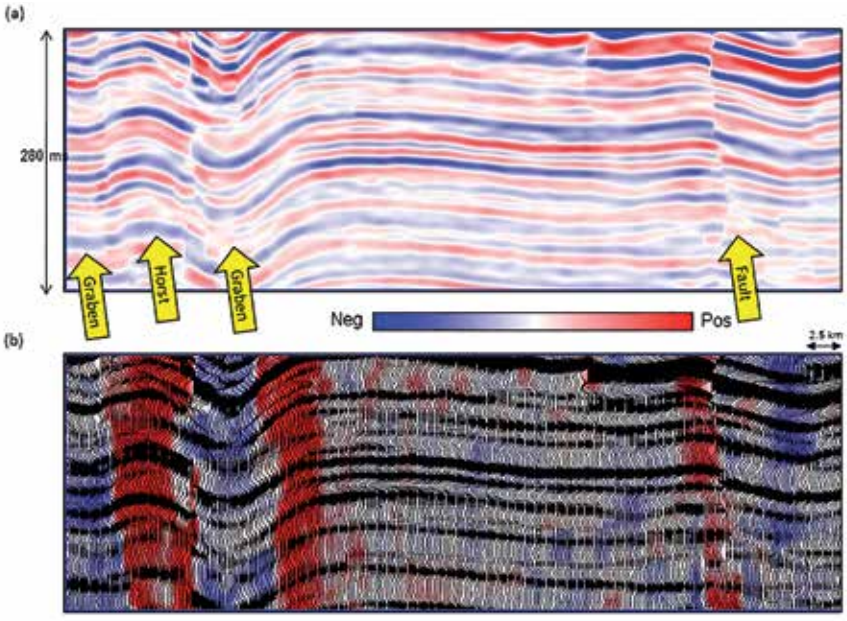

Figure 3 *(a) Vertical slice through seismic amplitude after structure-oriented filtering. Note the fault on the right and the horst and grabens on the left. (b) The same amplitude data displayed in wiggle and variable area co-rendered with most-positive and most-negative principal curvatures. The upthrown and downthrown sides of the fault exhibit a positive curvature (in red) and negative curvature (in blue) anomalies, consistent with the quarry outcrop image of conjugate faulting shown in Figure 2b. (Data courtesy: Arcis Seismic Solutions, TGS).*

of a normal fault, and a negative curvature anomaly with the downthrown side. The separation between the positive and the negative curvature lineaments would be a measure of the displacement of the fault. Similarly, the positive curvature will highlight the levees of an incised channel, and a negative curvature the thalweg of the channel. Figure 1b shows the difference between 'principal' curvatures and a simpler second derivative of the time-structure map. Almost all commercial software computes and all examples shown here will be of the two principal curvatures. Figure 2 is from Ferrill and Morris's (2008) careful study of faulting in Mesozoic carbonates expressing different geomechanical properties. This image shows several of the features common to curvature images. In this example, the hypothesized curvature on the footwall and hanging wall are due to a suite of conjugate faults that fall below the limits of seismic resolution. Furthermore, strain is transferred from one large fault to the other by means of relay ramps. Coherence would be insensitive to both the conjugate faults and the relay ramps but main faults are directly mapped. Using the two images together provides a fuller image of the deformation.

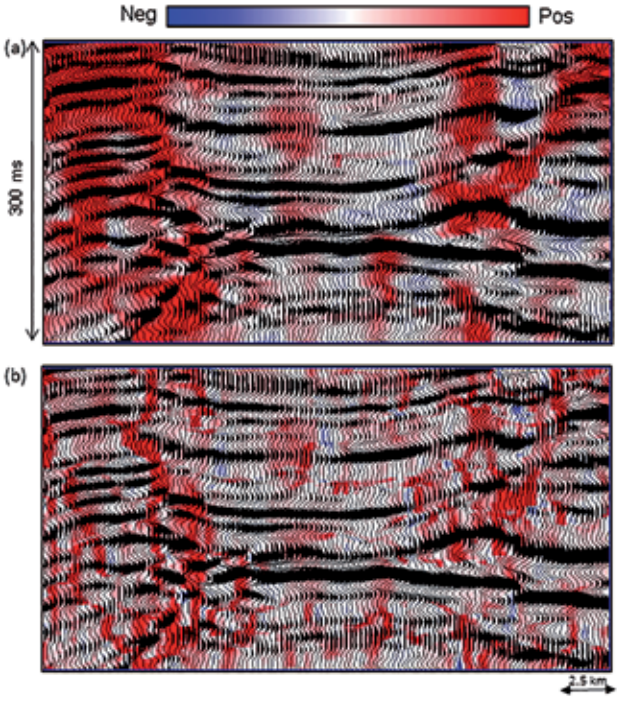

Figure 4 *A vertical slice through seismic amplitude co-rendered with (a) long-wavelength and (b) short-wavelength most-positive curvature. Blue zones indicate bowl-shape features. By construction, the longer wavelength image shows broader anticlines and synclines while the shorter wavelength images shows small kinks and flexures in the data. (Data courtesy: Arcis Seismic Solutions, TGS).*

Applications

In Figure 3 we overlay the most-positive principal curvature on a vertical slice through seismic amplitude. Note that the red colour correlates to positive folds or the upthrown sides of the faults. Al-Dossary and Marfurt (2006) introduced multi-spectral estimates of volumetric curvature with the intention of viewing the same geology at different scales. Here we show the most positive curvature long-wavelength (low-resolution) image and the short-wavelength (high-resolution) image in Figure 4 and the equivalent most-negative curvature long-wavelength and short-wavelength images in Figure 5. While the long-wavelength curvature image highlights the larger folds and flexures, the short-wavelength image highlights kinks and small offsets in the seismic reflectors. In Figure 6 we depict a comparison of time slices (close to t=1100 ms) through seismic amplitude, Energy-Ratio coherence, and the most-positive and most-negative curvature at long and short wavelengths. Note that the little kinks such as those seen in Figure 5 now take on meaning and indicate that some of these correspond to faults whose offset has fallen below the limits of seismic resolution. Yellow arrows

indicate further extent of a fault seen on coherence to the east. Given the strong positive curvature/coherence/negative coherence pattern, we are confident in saying the positive/negative curvature anomalies to the south (green arrows) indicate faults with very little offset.

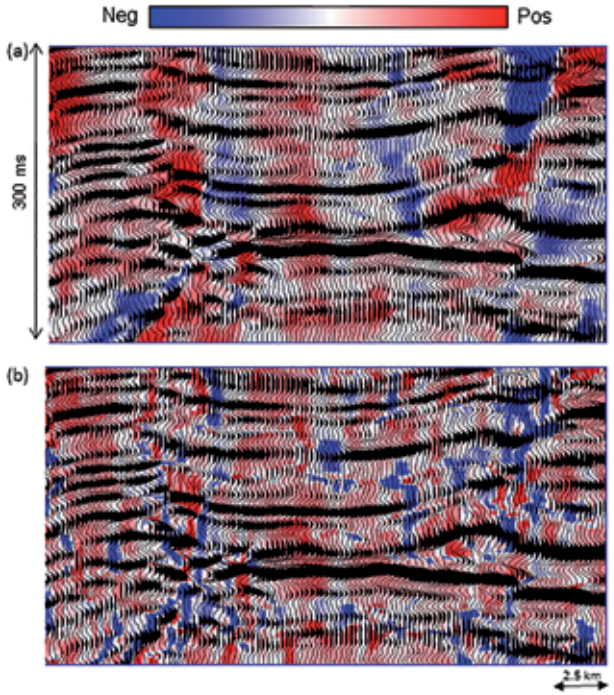

Figure 5 *A vertical slice through seismic amplitude co-rendered with (a) long-wavelength and (b) short-wavelength most-negative curvature. Red zones indicate dome-shaped features. By construction, the longer wavelength image shows broader anticlines and synclines while the shorter wavelength images shows small kinks and flexures in the data. (Data courtesy: Arcis Seismic Solutions, TGS).*

We exhibit a similar comparison in Figure 7 through another Canadian Western Sedimentary Province. Short-wavelength curvature anomalies are tightly correlated to faults delineated by coherence (yellow arrows) allowing us to extend our fault interpretation further to the NNE and SSW where the coherence anomalies die out. The more diffuse low coherence zones indicated by the green arrows indicate a rugose, tightly faulted and/or fractured horizon, which visually correlates to the long-wavelength curvature anticlines (in red) and synclines (in blue), which is readily seen by co-rendering the three images in Figure 7d. Geomechanically, such faulting and fracturing is often directly correlated to increased strain, measured by curvature. Depending on the geomechanical properties of the rocks, faults may appear as the quarry outcrop image shown in Figure 2d, exhibiting only a curvature anomaly. We use this analogue to explain the images shown in Figure 8 which shows horizon slices through a coherence and a most-negative principal curvature volume. There is sufficient displacement along several faults to give the coherence and curvature anomalies indicated by the yellow arrows. Such visual correlation validates our hypothesis that lineaments indicated by the green arrows in Figure 8b are also faults. We are confident that these anomalies are due to geology since these images were generated from a modern wide-azimuth, prestack time-migrated seismic amplitude data volume with careful surface-consistent statics. Often, however, we work with legacy data volumes

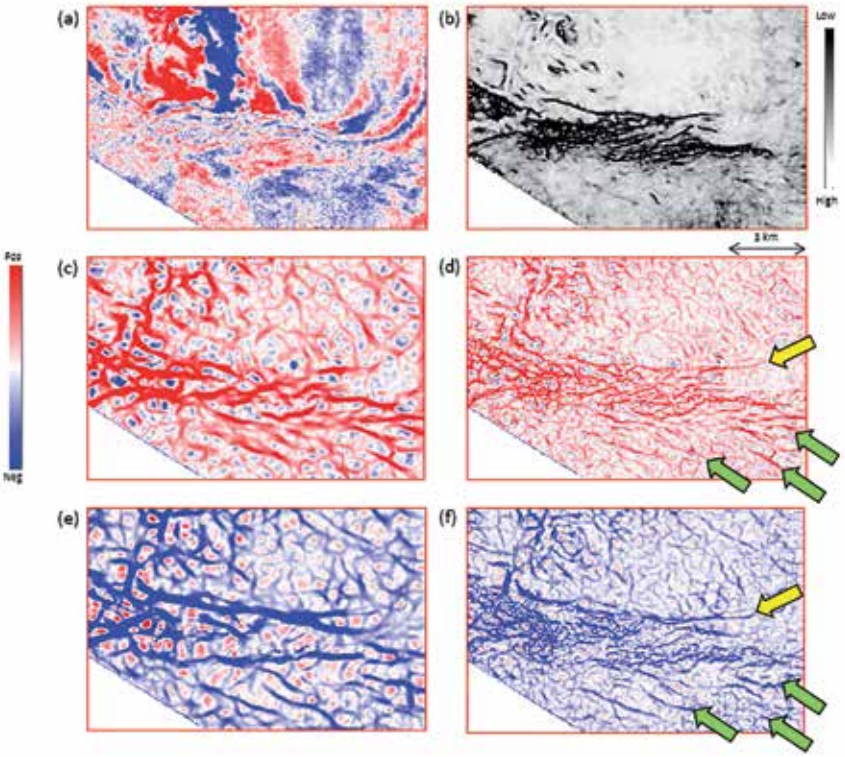

Figure 6 *The same times slice through (a) seismic amplitude, (b) coherence, (c) most-positive curvature (long-wavelength), (d) most-positive curvature (short-wavelength), (e) most-negative curvature (long-wavelength), and (f) most-negative curvature (short-wavelength). Notice that curvature extends the limits of faults beyond that seen in coherence both to the east and shows additional faults to the south. (Data courtesy: Arcis Seismic Solutions, TGS).*

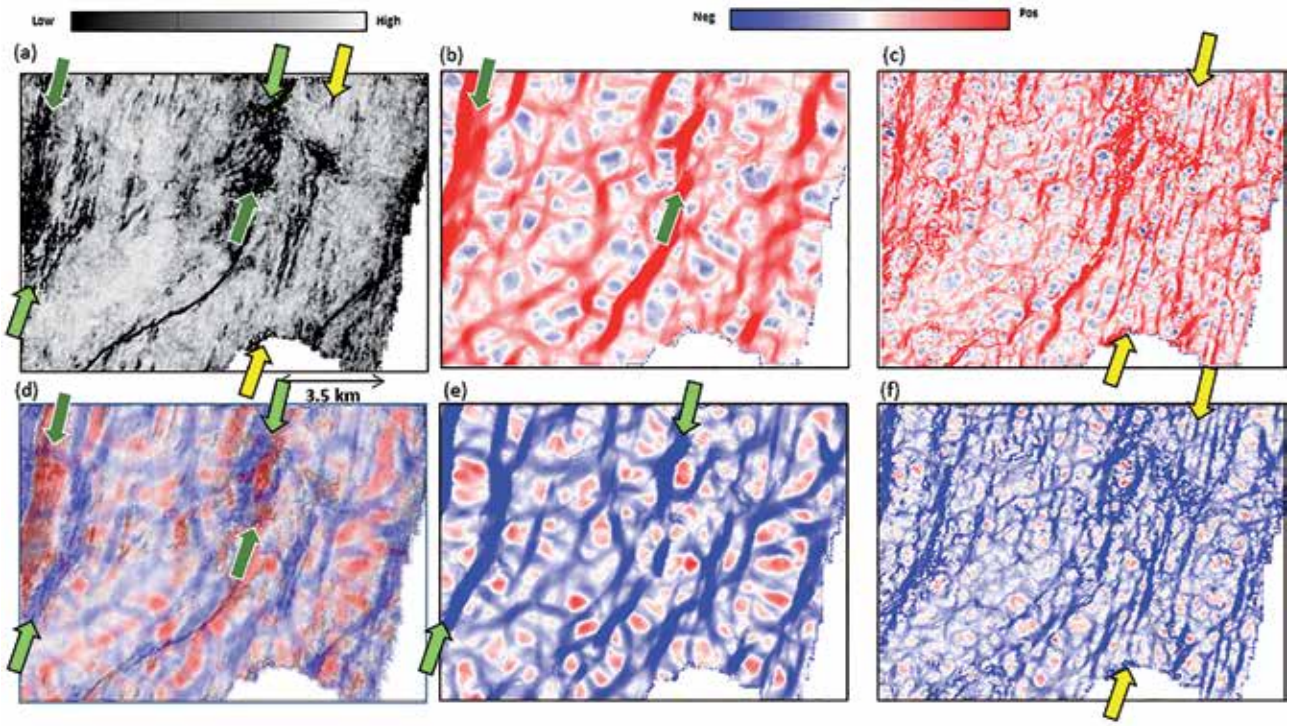

Figure 7 *Stratal slices through (a) coherence, (b) most-positive curvature (long-wavelength), (c) most-positive curvature (short-wavelength), (e) most-negative curvature (long-wavelength), and (f) most-negative curvature (short-wavelength). Note the complementary image of faults and flexures generated from coherence and the short wave curvature attributes, where the fault indicated by the yellow arrows loses offset it can no longer be seen in coherence but still exhibits curvature anomalies. (d) Co-rendered images of coherence and long wavelength curvature show that the strong incoherence anomalies indicating a rugose or highly faulted and fractured horizon (green arrows) are visually correlated to long wavelength synclines and anticlines which in turn measure areas of high strain. (Data courtesy: Arcis Seismic Solutions, TGS).*

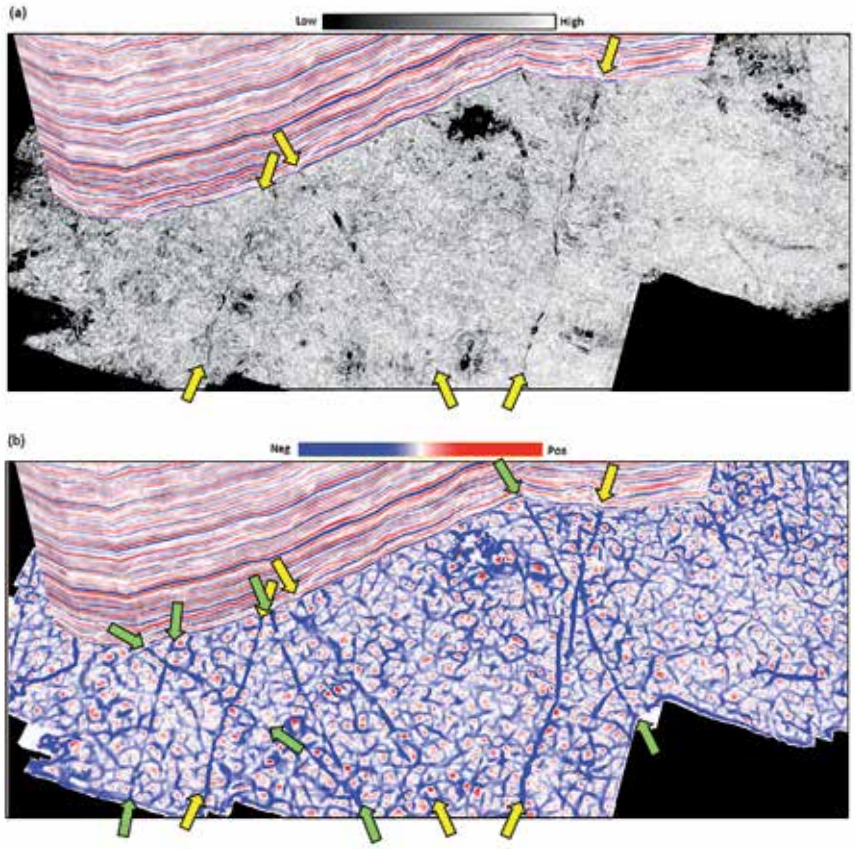

Figure 8 *Chair display showing a zig-zag seismic line through amplitude and a horizon slice through (a) coherence and (b) most-negative principal curvature. The lineaments on the coherence are correlated with their corresponding seismic amplitude signature. However, most of this image is high coherence and relatively featureless. In contrast, there is considerably more detail in the most negative curvature image. Correlating the curvature lineaments with those in coherence (the features indicated by yellow arrows) provides confidence in interpreting curvature lineaments without coherence anomalies to be faults with minimal vertical offset (the features indicated by green arrows). (Data courtesy: TGS).*

of lesser quality. In these situations, inferior statics, velocity analysis, and post-stack migration may give rise to smeared fault images. Such smeared fault images will produce a curvature anomaly but may not produce a coherence anomaly, even though the true fault has sufficient vertical displacement to be seen by properly processed data.

A similar comparison of coherence, most-positive and most-negative curvature is shown in Figure 9. There are only a few coherence anomalies, with co-rendering in Figure 9d showing them to be associated with anticlinal most-positive curvature anomalies. There are two potential interpretations here – complex folding giving rise to a suite of intersecting anticlines and synclines, or a suite of horsts and grabens that are faulted as in Figure 2d. The green arrows indicate strong coherence anomalies deeper in the section, supporting the latter faulting hypothesis.

Figure 10a shows a very clear image of faults delineated by coherence. However, by co-rendering the coherence with the most-positive and most-negative curvature images in Figure 10b we see that these faults delineate a suite of horsts

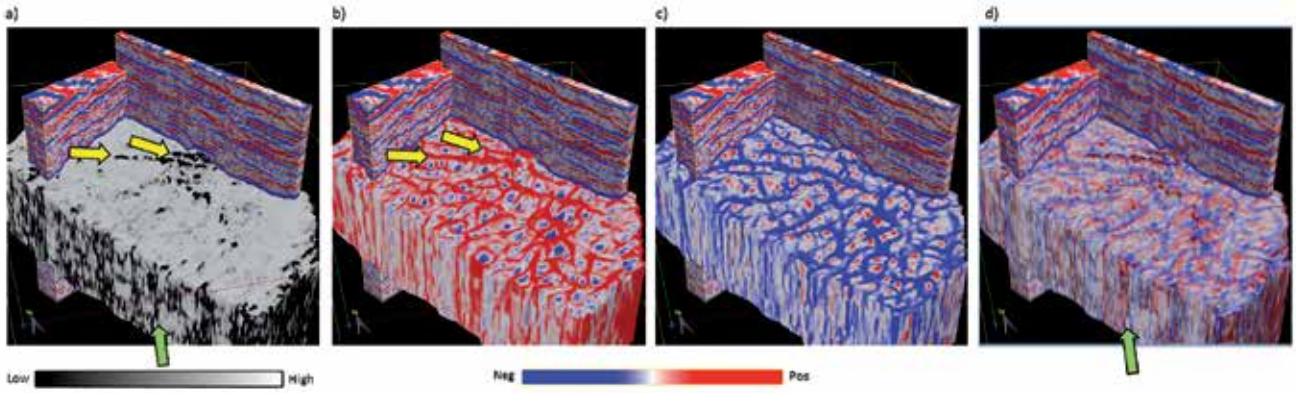

Figure 9 *Seismic sub-cubes shown intersecting a strat-cube from (a) coherence volume, and long-wavelength (b) most positive and (c) most negative curvature volumes. (d) Co-rendering of the three volumes. In this example, the coherence anomaly correlates with the anticlinal curvature anomalies (yellow arrows). Along this horizon the rocks either fold or deform as in Figure 2b, with very little vertical offset that can be measured by coherence. The green arrows indicate strong coherence anomalies deeper in the section, supporting the latter faulting hypothesis. (Data courtesy: Arcis Seismic Solutions, TGS).*

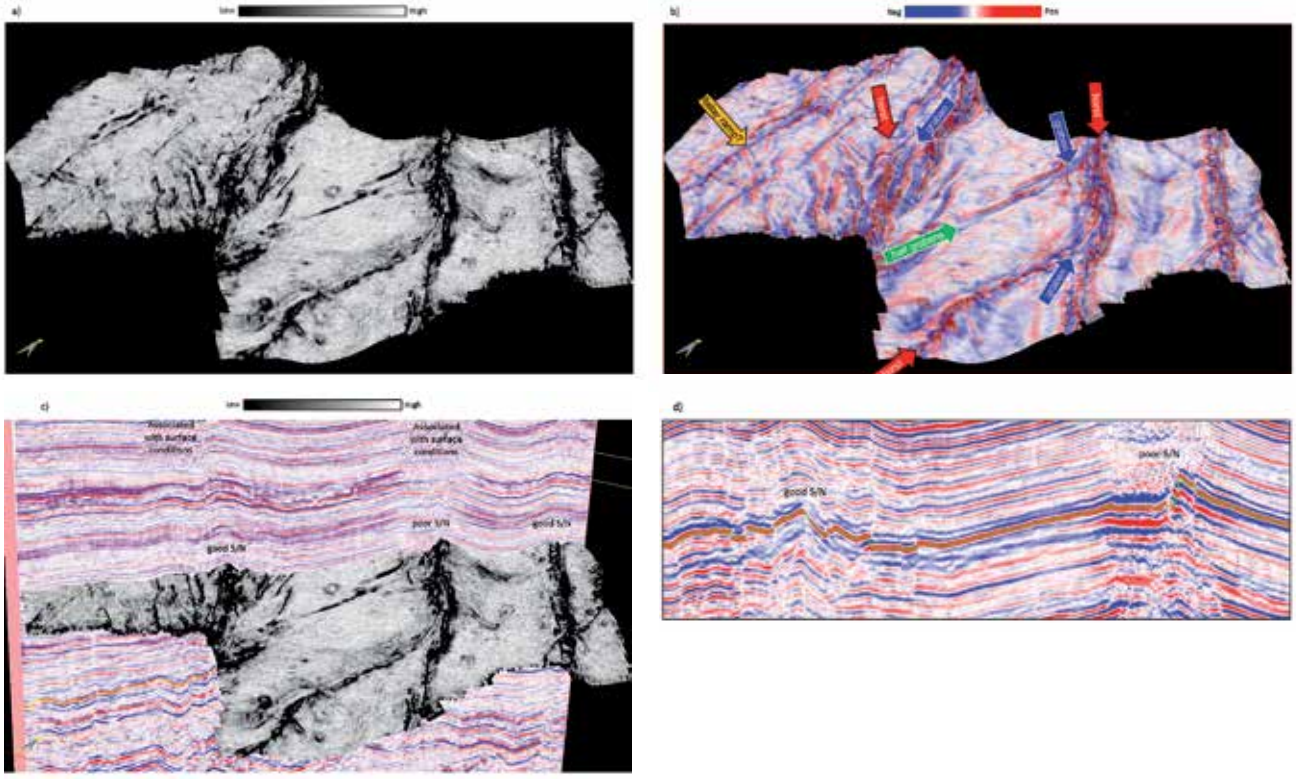

Figure 10 *Stratal cube through (a) coherence and (b) co-rendered coherence and most positive and most negative curvature volumes. While the coherence clearly delineates a number of faults, curvature provides a complementary display of horsts and grabens. (c) and (d) Note strong coherence anomalies correlated with the horst blocks. Examination of the seismic amplitude shows good signal-to-noise over two of the horst blocks suggesting a highly faulted, rugose surface, and poor signal-to-noise over the centre horst block. The noisy shallow part of (c) is not due to poor imaging of steep dips, but due to surface conditions associated with the deeper structure. (Data courtesy: Arcis Seismic Solutions, TGS).*

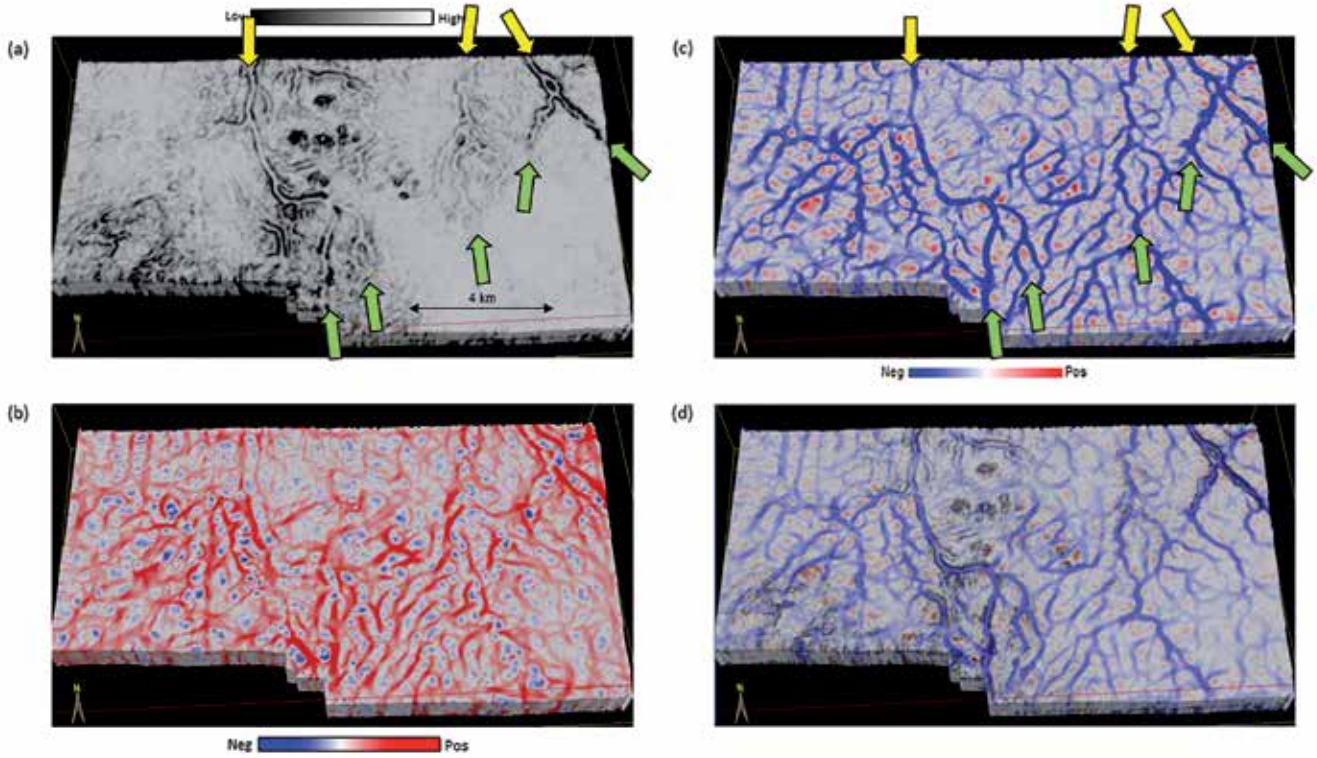

Figure 11 *Stratal cube through the (a) coherence, (b) most positive curvature, and (c) most negative curvature volumes. (d) Co-rendered image of all three attributes. Yellow arrows delineate channel edges seen in coherence. Notice that these channels can be followed further on the most negative curvature image. We interpret the negative curvature anomaly to be due to differential compaction over shale-filled channels. (Data courtesy: Arcis Seismic Solutions, TGS).*

and grabens. In this example the three attributes provide complementary images, where one is not 'better' than the other. Using Figure 2c as an analogue, we anticipate the existence of relay ramps linking the major fault systems.

Figure 11 further illustrates the complementary nature of curvature and coherence. Energy-ratio coherence seen in Figure 11a delineates three distributary channels. As the channels bifurcate, they become progressively narrower and thinner, eventually falling below tuning where the waveform becomes constant and the coherence anomaly ends (indicated by green arrows). The most-positive curvature shows the flanks of the channels as well as potential levees, while the most negative curvature shows the channel axes (thalwegs). The yellow and green arrows shown in Figure 11a are redisplayed on Figure 11c. Note how one can follow these distributary channels as they continue to bifurcate. Co-rendering coherence and most-negative curvature in Figure 11d provides a one-to-one correlation between coherence edges and channel axises where the channels are relatively thick, thereby validating our hypothesis that the curvature anomalies correlate to channels even though the coherence channel edge anomalies disappear. We interpret these negative curvature anomalies to be due to differential compaction of softer channel fill, probably shale, incised within a firmer flood-plane matrix.

Figures 12 and 13 show channels from two different surveys that exhibit the opposite behaviour, with the channels

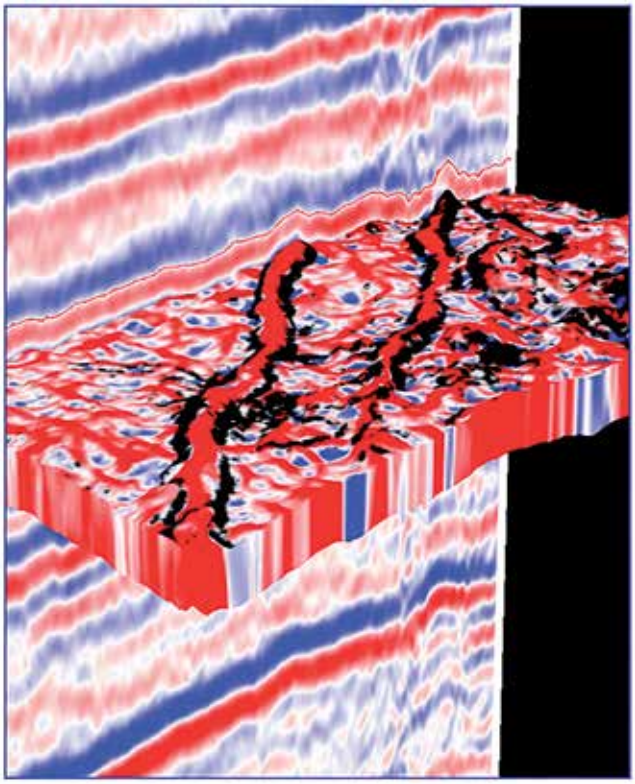

Figure 12 *A vertical slice through seismic amplitude and a stratal-cube of most-positive curvature co-rendered with coherence seen here in a 3D chair view. (Data courtesy: Arcis Seismic Solutions, TGS).*

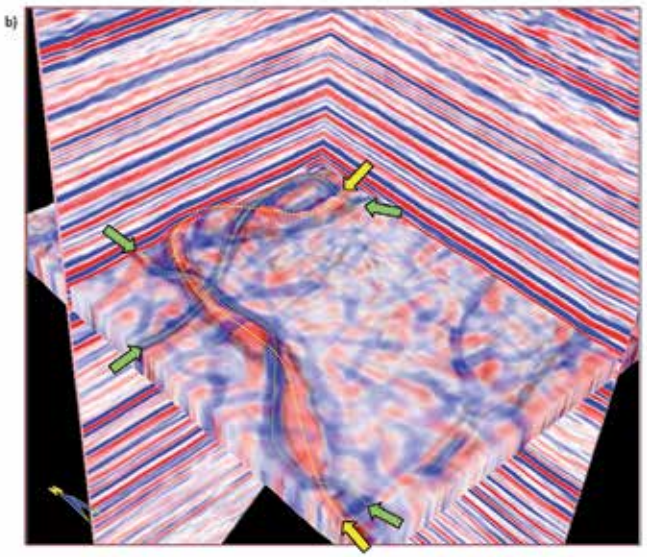

Figure 13 *Strat-cube of (a) coherence and (b) co-rendered coherence and most positive most negative curvature. Yellow arrows indicate a wide channel with a positive curvature anomaly while green arrows indicate several narrow channels with negative curvature anomalies. Such differential compaction is a lithology indicator, with positive features suggesting a sand-filled channel and negative features shale-filled channels. (Data courtesy: Arcis Seismic Solutions, TGS).*

appearing as topographic highs giving rise to a most-positive curvature anomaly (in red) delineated by channel edges seen in coherence. In both cases we interpret the channels to be sand-filled, having undergone less differential compaction than the flood plane. In these cases, the curvature anomalies not only confirm the channel image seen in coherence, but also provide a lithology indicator.

Euler curvature

Just as one can measure apparent dip in a given direction, one can measure apparent curvature, the latter of which is referred to as Euler curvature. The true dip is the apparent dip with the greatest magnitude. Similarly, most-positive and most-negative curvature define the magnitude and direction of apparent curvature having the most positive and most negative magnitude. As shown in the previous images, faults and flexures of all directions are measured by most-positive and most-negative curvature. If we have additional information, such as natural fractures seen on image logs, we may wish to only illuminate the apparent curvature correlated with these natural fractures (Chopra and Marfurt, 2013). Euler curvature is run on post-stack seismic volumes and can therefore highlight an interpreter-defined set of lineaments of interest. Figure 14 shows stratal slices through Euler curvature striking -90^0, -45^0, 0^0 and 45^0 as well as coherence. If the present-day stress were to indicate that EW-trending flexures were correlated with open fractures, one could correlate the intensity of Euler curvature seen in the -90^0 image to production. Note lineaments are not seen in this direction on coherence. Depending on the desired level of detail, the long- or the short-wavelength computations can be resorted to. For

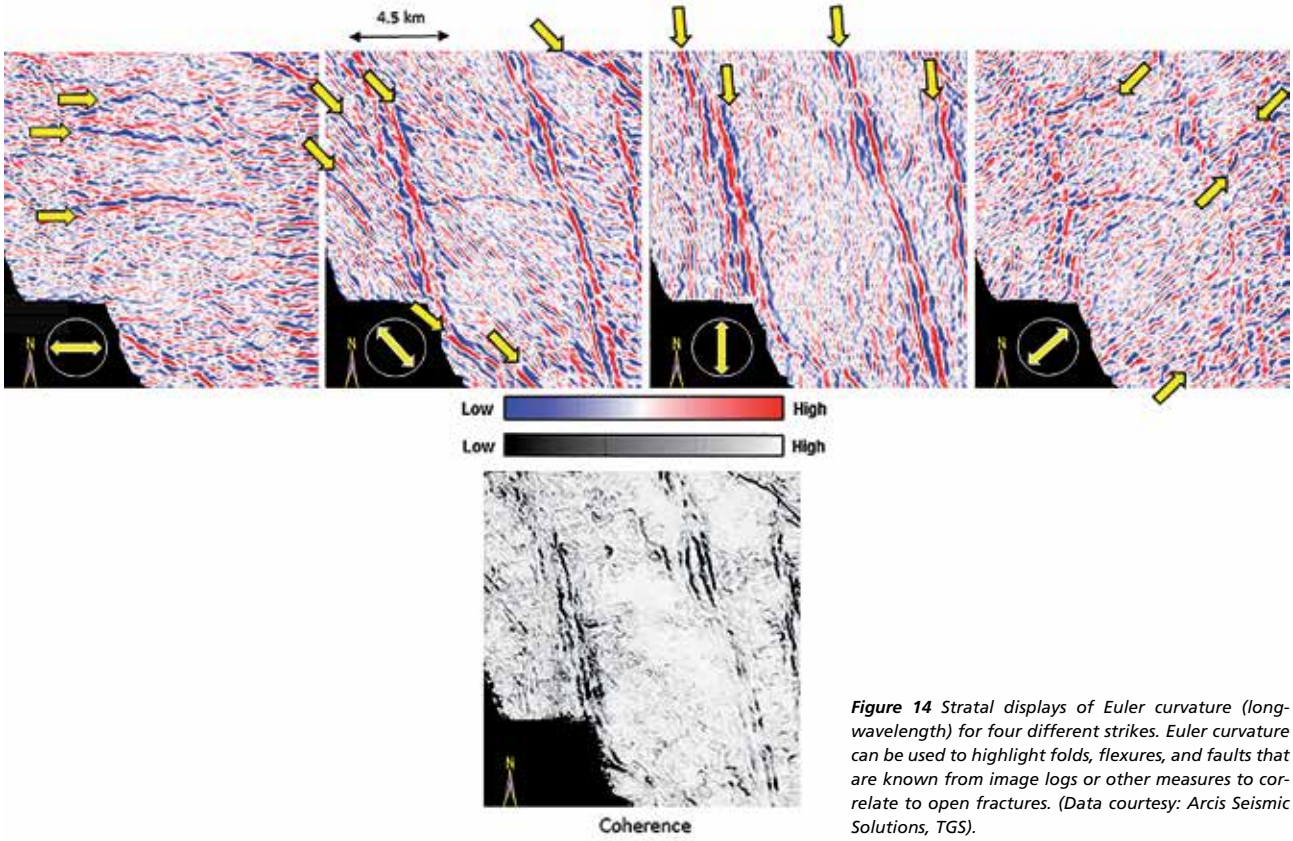

Figure 14 *Stratal displays of Euler curvature (long-wavelength) for four different strikes. Euler curvature can be used to highlight folds, flexures, and faults that are known from image logs or other measures to correlate to open fractures. (Data courtesy: Arcis Seismic Solutions, TGS).*

observing fracture lineaments the short-wavelength Euler curvature would be more beneficial.

Interpretation of lineaments from curvature displays

Mathematically, curvature is an eigenvalue/eigenvector problem. For a hypothesized 2D surface residing in a 3D volume, the most-positive and most-negative curvatures are the eigenvalues. The corresponding eigenvectors provide the strike of these curvature lineaments. Thus, at every voxel we have a measure not only of the amount of deformation, but also of its directions. The strike of most-positive and most-negative curvature was used to construct the previous Euler curvature volumes. They can also be used to generate a rose diagram, as shown in Figure 15, and calibrated to rose diagrams computed from image logs. The length of each petal of the rose is dependent on the frequency of lineaments falling along any angle. Such rose diagrams can then be compared with similar rose diagrams that are obtained from image logs to gain confidence in the seismic-to-well calibration (Rao et al., 2009). Once a favourable match is obtained, the interpretation of fault/fracture orientations and the thicknesses over which they extend can be used with greater confidence for more quantitative reservoir analysis. Such calibrations may be carried out in localized areas around the wells for accurate comparisons.

Chopra et al. (2009), discuss the generation of 3D rose diagrams from the attribute volumes, which can not only be calibrated with the recorded borehole image logs, but also visualized for gaining more information such as azimuthal anisotropy in the broad zone of interest. Such rose diagrams are generated on a gridded square area defined by an n-inline by m-crossline analysis window, for each horizontal time slice. Within each analysis window, each pixel is binned into rose petals according to its strike, ψ, weighted by its threshold-clipped ridge or valley components of curvedness (determined from the minimum and maximum curvature), then sum and scale them into rose diagrams. The process is repeated for the whole data volume. After that, the rose diagrams are mapped to a rose volume which is equivalent to the data volume and centered in the analysis window, located at the same location as in the input data volume. A robust generation of rose diagrams for the whole lineament volume (corresponding to the seismic volume) is computed, yielding intensity and orientation of lineaments. Such a volume can be merged with any other attribute volume that has been generated to study the fracture lineaments and their orientation.

Attempts have been made by different workers to make use of curvature and other attributes for more accurate interpretations. Rather than map the intensity of the strongest attribute lineaments, Singh et al. (2008), used an image-processing (ant-tracking) algorithm to enhance curvature and coherence lineaments that were parallel to the strike of open fractures, at an angle of some 45^0 to the strike of

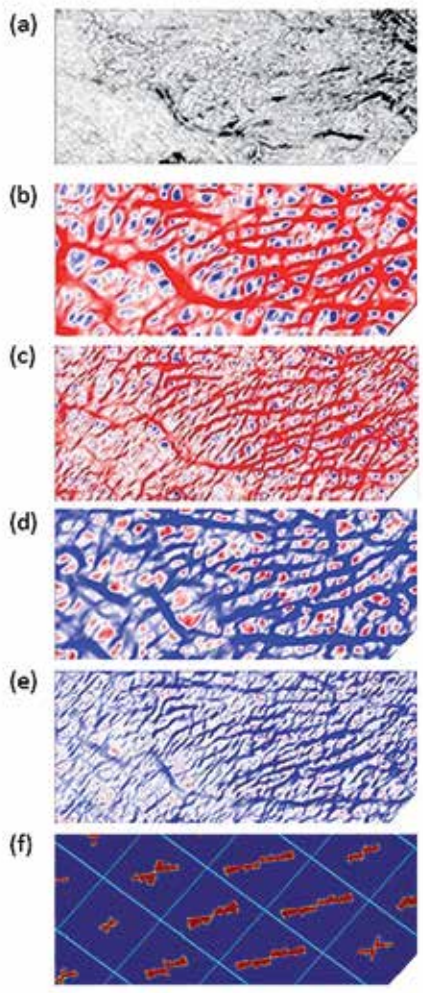

Figure 15 *Time slices (at t=2418 ms) through (a) coherence, (b) most-positive curvature (long-wavelength), (c) most-positive curvature (short-wavelength), (d) most-negative curvature (long-wavelength), and (e) most-negative curvature (short-wavelength) volumes. Corresponding time slice through the 3D rose volume. Notice, the density and orientation of lineaments on the attributes is represented clearly on the rose diagrams. (Data courtesy: CGGVeritas Library Canada).*

the strongest lineaments. Henning et al. (2010), use related technology to azimuthally filter lineaments in the Eagle Ford formation of south Texas. They then compute RMS maps of each azimuthally-limited volume that can be correlated to production (Guo et al (2010), and hypothesize that each azimuthally-limited attribute volume computed from k_1 and ψ_1 corresponds to open fractures. Each of these volumes is then correlated to production to either validate or reject the hypothesis.

Ant-tracking and other image processing tools have become popular in estimating discrete fracture networks. The most common application is to the coherence family of attributes, such as variance. However, any attribute that provides lineament anomalies can be subjected to such image processing. Re-examining Figure 1b, we recognize that in the case of curvature, the 'ants' track axial planes rather than discontinuities. Figure 16 shows such an

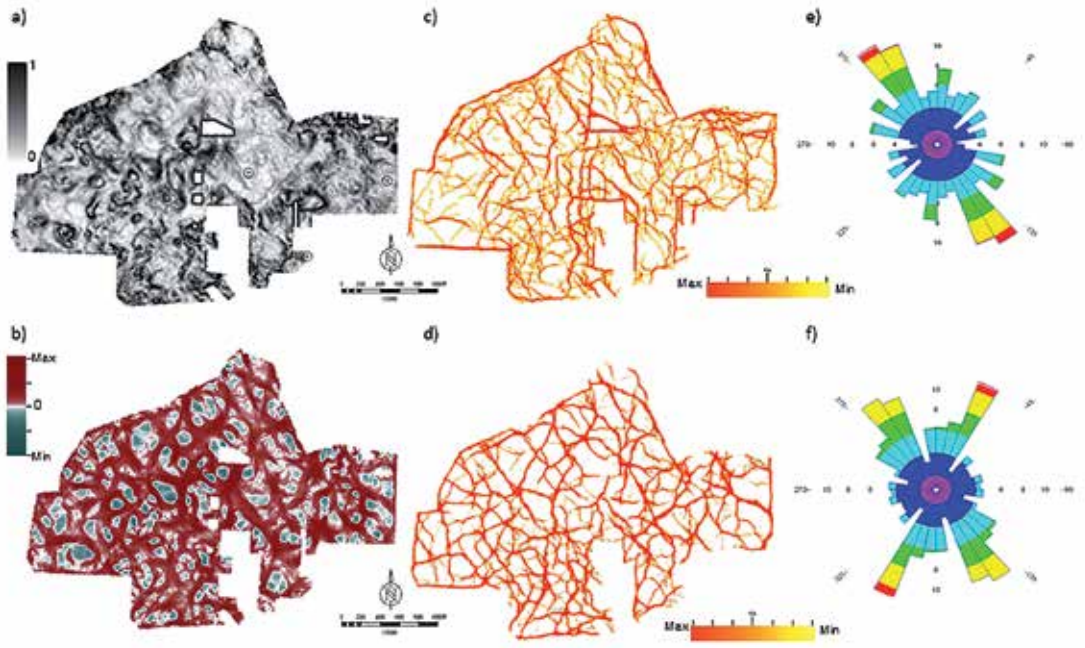

Figure 16 *Stratal slices along the base Barnett Shale through (a) variance volume, and (b) principal most-positive curvature volume. Corresponding stratal slices through ant-tracked volumes of (c) variance and (d) most positive curvature. (e) and (f) show the rose diagrams prepared from lineaments shown in (c) and (d) respectively. Notice, there are two main axises in the curvature rose diagram and only one in the variance diagram. (Modified from Baruch, 2009, Data courtesy of Devon Energy).*

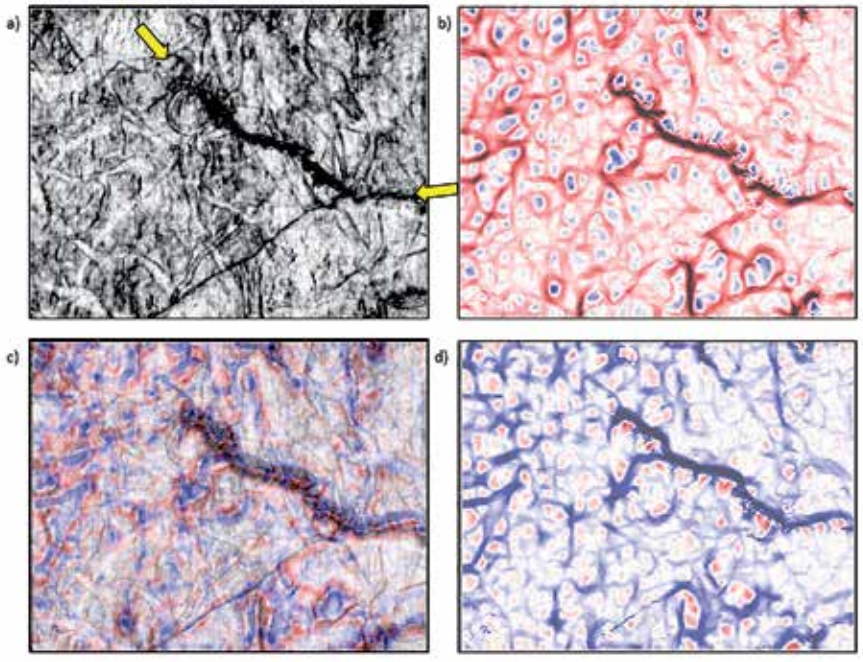

Figure 17 *An example where curvature is 'overrated' showing phantom horizon slices through (a) Sobel filter 'coherence', (b) most-positive curvature, and (d) most-negative curvature volumes for data acquired on the Gulf of Mexico shelf. (c) Co-rendered image of the three attributes. Note that other than an image of the larger listric fault (yellow arrows), the curvature images give little indication of the channels that are clearly defined by coherence.*

application to a Barnett Shale survey. In many parts of the Barnett Shale, structural ridges delineated by most positive curvature are diagenetically strengthened and are barriers to hydraulic fractures – with microseismic data occurring in bowls (Trumbo and Rich, 2013). Note that these ridges are clearly delineated by most positive curvature (Figure 16b) giving rise to a network of ant-tracked lineaments. In contrast, the variance volume is dominated by the NW-SE trending lineaments.

A case where curvature is 'overrated'

The astute reader may have noticed that all but one of the previous examples have come from the Western Canadian Sedimentary Province while the last example came from the Fort Worth Basin of Texas. All these examples are of Mesozoic and Paleozoic sediments that have gone through a great deal of lithification. Figure 17 shows an example like those provided by Barnes (2014). This example from South Marsh Island, Louisiana, offshore Gulf of Mexico is

represented by a spaghetti-like collection of fluvial channels, each one cutting into its deeper predecessors. Inspecting these images shows that other than the correlation of curvature about the major listric fault indicated by yellow arrows, there is little correlation to the channels clearly seen in the Sobel filter coherence image. Specifically, we do not recognize the clear differential compaction anomalies seen in Figures 11-13. This failure of curvature to delineate channels is common to many Tertiary Basin surveys. These channels do indeed undergo differential compaction, some with positive anomalies (suggesting sand fill), and some with negative anomalies (suggesting shale fill). However, the compaction effect is cumulative, with all deeper anomalies contributing to the image seen on this phantom horizon slice. Other workers have addressed this problem by first flattening on a horizon below the zone of interest, thereby palinspastically removing deeper compaction effects. Unfortunately, this data volume is so channelized that there is no such deeper horizon to pick, and the promise of curvature is overrated.

Conclusions

Coherence and curvature are complementary attributes that define tectonic deformation including faulting and folding as well as incisement, collapse, and differential compaction of stratigraphic horizons. In general, coherence and curvature should be used together, either through co-rendering or animation. In most cases, curvature images are complementary to coherence images, adding additional insight to the same geologic features. In many cases, one can 'calibrate' curvature anomalies to more familiar coherence anomalies, allowing one to extend the interpretation of faults that lose throw or channels that lose thickness beyond the limits of the coherence anomalies. Curvature measures strain, and thus, along with lithology and thickness, serves as an indicator of zones amenable to natural fractures. When there is differential compaction over channels, curvature can also be used as a lithologic indicator.

Interpreters working a given geologic province or evaluating a given geologic feature will quickly learn whether coherence, curvature, or any attribute adds value to their interpretation. Instead of searching for the best attribute and getting into a debate of an attribute being overrated or not, we recommend the complimentary application of these attributes for interpretation of seismic data. This aspect is very important and we feel it should not be overlooked.

Acknowledgements

We wish to thank Arcis Seismic Solutions, TGS, Calgary, Canada for encouraging this work and for permission to present these results.

References

Al-Dossary, S. and Marfurt, K. J. [2006] 3-D volumetric multispectral estimates of reflector curvature and rotation. *Geophysics*, **71**, 41–51.

Bahorich, M.S. and Farmer, S.L. [1995] 3D seismic coherency for faults and stratigraphic features. *The Leading Edge*, **14**, 1053–1058.

Bakker, P. [2003] Image structure analysis for seismic interpretation. Ph.D. thesis, Technische Universiteit Delft.

Barnes, A.E. [2014] Is curvature overrated? *First Break*, 32, 65-69.

Baruch, E., Elebiju, O. and Perez, R. [2009] Geophysical evidence of basement controlled faulting in the Ellenburger Group and Viola Limestone, Fort Worth Basin, Texas: 79th Annual International Meeting Society of Exploration Geophysicists, Expanded Abstracts, 995-999.

Chopra, S. and Marfurt, K. J. [2008] Gleaning meaningful information from seismic attributes. *First Break*, **26**, 43-53.

Chopra, S., Marfurt, K.J. and Mai, H.T. [2009] Using automatically generated 3D rose diagrams for correlation of seismic fracture lineaments with similar lineaments from attributes and well log data. *First Break*, 37-42.

Chopra, S. and Marfurt, K. J. [2013] Observing fracture lineaments with Euler curvature. *The Leading Edge*, **32**, 122-126.

Ferrill, D.A. and Morris, A.P. [2008] Fault zone deformation controlled by carbonate mechanical stratigraphy, Balcones fault system, Texas. *AAPG Bulletin*, **92**, 359-380.

Gersztenkorn, A. and Marfurt, K.J. [1999] Eigenstructure-based coherence computations as an aid to 3D structural and stratigraphic mapping. *Geophysics*, **64**, 1468–1479.

Guo, Y., Zhang, K. and Marfurt, K.J. [2010] Seismic attribute illumination of Woodford Shale faults and fractures, Arkoma Basin, OK: 80th Annual International Meeting, SEG, Expanded Abstracts, 1372–1376.

Henning, A.T., Martin, R., Paton, G. and Kelvin, R. [2010] Data conditioning and seismic attribute analysis in the Eagle Ford Shale Play: Examples from Sinor Ranch, Live Oak County, Texas: 80th Annual International Meeting, SEG, Expanded Abstracts, 1297–1301.

Luo, Y., al-Dossary, S., Marhoon, M. and Alfaraj, M. [2003], Generalized Hilbert transform and its application in geophysics. *The Leading Edge*, **22**, 198-202.

Luo, Y., Higgs, W.G. and Kowalik, W.S. [1996] Edge detection and stratigraphic analysis using 3D seismic data: 66th Annual International Meeting, SEG, Expanded Abstracts, 324–327.

Mai, H.T., Marfurt, K.J. and Chávez-Pérez, A.S. [2009] Coherence and volumetric curvatures and their spatial relationship to faults and folds, an example from Chicontepec Basin, Mexico: 79th Annual International Meeting of the SEG, Expanded Abstracts, 1063-1067.

Marfurt, K.J., Kirlin, R.L., Farmer, S.H. and Bahorich, M.S. [1998] 3D seismic attributes using a running window semblance-based algorithm. *Geophysics*, **63**, 1150–1165.

Rao, S.N., Al-Kandari, A.L., Kidambi, V.K., Al-Ashwak, S., Al-Qadeeri, B. and Pattnaik, C. [2009] Understanding fractures through seismic data: North Kuwait case study, SEG Expanded Abstracts, 547-551.

Singh, S.K., Abu-Habbiel, H., Khan, B., Akbar, M., Etchecopar, A. and Montaron, B. [2008] Mapping fracture corridors in naturally fractured reservoirs: an example from Middle East carbonates. *First Break*, **26**, 109-113.

Trumbo, A. and Rich, J.P. [2013] Azimuthal variations in attributes for induced fracture detection in the Barnett Shale. *Interpretation*, **1**, (2), SB51–SB59.

Received 16 October 2014; Accepted 3 November 2014.
Doi: 10.3997/1365-2397.2014021

